Optical interface engineering with on-demand magnetic surface conductivities

Yuhan Zhong,[1,2] Tong Cai,[1,2] Tony Low,[3,*] Hongsheng Chen,[1,2,†] and Xiao Lin[1,2,‡]

[1]*Interdisciplinary Center for Quantum Information, State Key Laboratory of Modern Optical Instrumentation, ZJU-Hangzhou Global Scientific and Technological Innovation Center, College of Information Science and Electronic Engineering, Zhejiang University, Hangzhou 310027, China*

[2]*International Joint Innovation Center, ZJU-UIUC Institute, Key Lab. of Advanced Micro/Nano Electronic Devices & Smart Systems of Zhejiang, The Electromagnetics Academy at Zhejiang University, Zhejiang University, Haining 314400, China*

[3]*Department of Electrical and Computer Engineering, University of Minnesota, Minneapolis, Minnesota 55455, USA*

(Received 2 August 2021; revised 15 June 2022; accepted 30 June 2022; published 11 July 2022)

Optical interfaces with arbitrary magnetic and electric surface conductivities can enable the design of photonic devices with new functionalities, but practical approaches to date are nonexistent. Regular interfaces, such as those with graphene, are optically interesting due to their tailorable electric surface conductivity. However, their magnetic surface conductivity is negligible since the magnetic response in natural materials is generally weak from the terahertz frequency onward. The quest for artificial magnetic response has recently triggered the development of magnetic metasurfaces that, however, can only provide the interface with a limited value of magnetic surface conductivity. Herein we find that vertical heterostructures based on regular *nonmagnetic* metasurfaces have a direct correspondence to an optical interface with both magnetic and electric surface conductivities, whose desired values can be structurally engineered. Moreover, we identify several unique photonic and plasmonic responses at optical interfaces with specific magnetic surface conductivities, including a polarization-insensitive Brewster effect and pure magnetic surface waves.

DOI: 10.1103/PhysRevB.106.035304

I. INTRODUCTION

In many instances in material science, "the interface is the device" [1,2]—an observation that is particularly true in photonics and most notably with the advent of metasurfaces and two-dimensional (2D) materials. In general, the optical interface can be characterized with magnetic (σ_m) and/or electric (σ_e) surface conductivities [3–5]. From the duality principle, magnetic and electric surface conductivities are of equal importance since they control the character (e.g., wave front, polarization, magnitude) [6–11] of electromagnetic waves, and their prudent design can allow for beam shaping, steering, and focusing [12–16]. As such, there is a continuing quest to realize optical interfaces with desired values of magnetic and electric surface conductivities.

However, for conventional optical interfaces (such as those with graphene, a typical 2D material), they generally only have an electric surface conductivity [17–22], while their magnetic surface conductivity is almost zero, due to the weak magnetic response in natural materials. As a result, for optical interfaces, their intriguing physics and applications have been limited to cases only with electric surface conductivity, while cases with magnetic surface conductivity have remained largely unexplored, even in theory. Recent approaches to inducing a finite magnetic response at the interface resort to magnetic metasurfaces. The magnetic metasurfaces use resonant geometries with rather complex, deep-subwavelength irregular patterns, e.g., split-ring resonators, fishnet structures, and nanoparticle arrays [9–16,23,24]. In principle, a strong magnetic response can be created through displacement or conduction currents within the magnetic metasurface. However, these deep-subwavelength irregularities unavoidably pose difficulty and challenges in the fabrication process, along with complexity in theoretical modeling. Despite the considerable advances in magnetic metasurfaces, the reported achievable values of magnetic surface conductivity are still limited. A general strategy to engineer giant and even on-demand magnetic surface conductivities would present a fundamental breakthrough in the advancement of photonics.

Here, we propose a universal scheme to design optical interfaces with on-demand magnetic surface conductivities, whose value—in principle—can be unbounded. We motivate our approach by first establishing a direct equivalence between magnetic optical interfaces and vertical heterostructures. Note that for regular vertical heterostructures, especially those composed of regular nonmagnetic metasurfaces and dielectric slabs, their optical response is generally considered nonmagnetic [17–22]. However, upon close inspection, we reveal that these vertical heterostructures are, in fact, equivalent to an optical interface characterized by effective magnetic and electric surface conductivities. Remarkably, the magnetic surface conductivity can be readily tailored, for example, through the thickness a of dielectric slabs and the electric surface conductivity σ_s of nonmagnetic metasurfaces. This scheme then facilitates the exploration of intriguing physics and applications of optical interfaces with magnetic surface conductivity, such as transverse electric (TE, *s*-polarized)

*tlow@umn.edu
†hansomchen@zju.edu.cn
‡xiaolinzju@zju.edu.cn

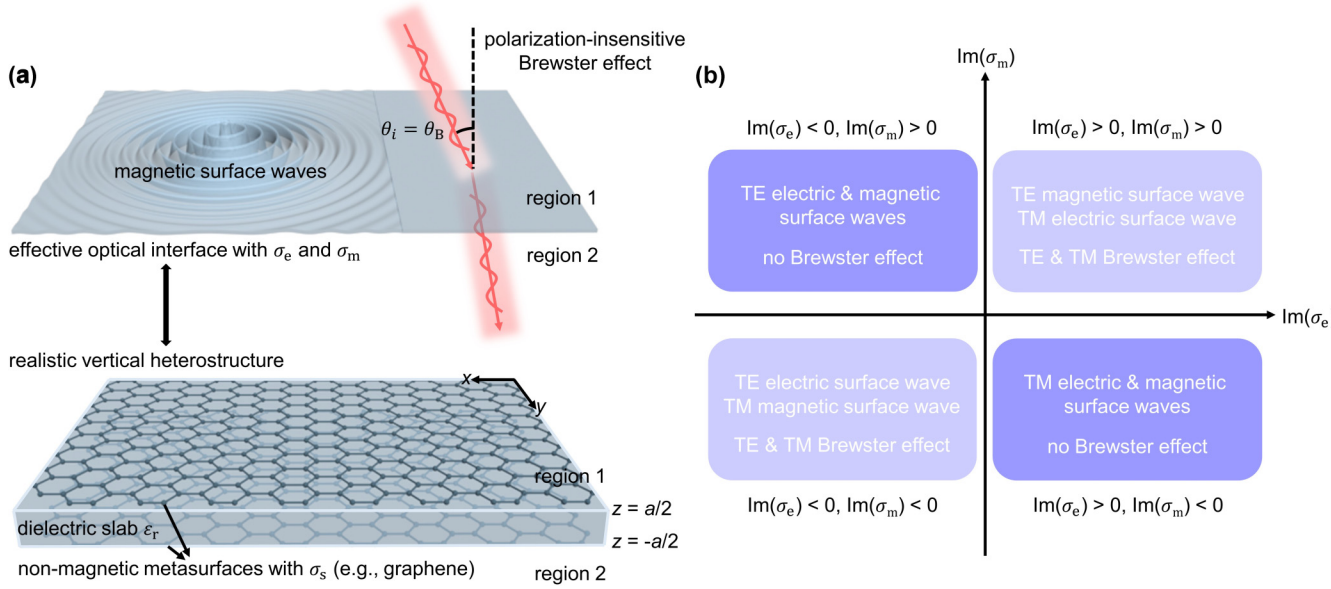

FIG. 1. Exotic photonic and plasmonic responses at the optical interface with on-demand magnetic surface conductivities. (a) Schematic illustration of the effective optical interface with magnetic and electric surface conductivities, which are denoted as σ_m and σ_e, respectively. Such an optical interface (upper panel) can be effectively constructed by a vertical metasurface–dielectric–metasurface heterostructure (lower panel), in which the metasurface (e.g., graphene) is nonmagnetic. For conceptual illustration, the figure in (a) is not plotted to scale; actually, the distance between the two parallel interfaces is much larger than the C—C bond length in graphene. (b) Existence of Brewster effect and surface waves in the parameter space of Im(σ_e) and Im(σ_m). Here, and in the following figures, the regions above (region 1) and below (region 2) the optical interface are both free space.

or transverse magnetic (TM, *p*-polarized) magnetic surface waves and a polarization-insensitive Brewster effect. The polarization-insensitive Brewster angle can vary from 0° to 90° by engineering the ratio between electric and magnetic surface conductivities. Moreover, we find the transmittance through an optical interface with $\sigma_e \to \infty$ can gradually increases from zero to unity by increasing σ_m.

II. RESULTS AND DISCUSSION

We begin with the introduction of a universal scheme to construct effective optical interfaces with a magnetic surface conductivity by exploiting vertical heterostructures. The vertical heterostructure is composed of a dielectric slab sandwiched between two identical *nonmagnetic* metasurfaces [Fig. 1(a)]. The dielectric slab has a relative permittivity of ε_r (e.g., $\varepsilon_r = 2$ used in the calculation) and a thickness of a. For the sake of simplicity, the regions above and below the dielectric slab are both set to be free space. The only assumption used in the derivation is that these nonmagnetic metasurfaces in Fig. 1(a), such as graphene and metal-based nanostructures, can be effectively treated as a homogenized interface and modeled by an electric surface conductivity σ_s [17–22]. The homogenization of these metasurfaces is generally reasonable, if the size of their unit cells is much smaller than the wavelength of the studied waves, including propagating waves and surface waves. Meanwhile, this work is carried out under the scenario that the distance between these two metasurfaces is much larger than the bond length in their constitutive materials (e.g., the C—C bond length in graphene).

After some calculations (Supplemental Material Sec. S1 [25]), the vertical heterostructure is found to be equivalent to an optical interface with an effective magnetic surface conductivity σ_m^{TE} (σ_m^{TM}) and electric surface conductivity σ_e^{TE} (σ_e^{TM}) for TE (TM) waves. These surface conductivities can be derived by following a similar calculation procedure in Ref. [26]. In short, they can be expressed as

$$\sigma_m^{\mathrm{TE}} = \frac{\omega\mu_0\left(e^{ik_z^{\mathrm{diel}}a/2} - e^{-ik_z^{\mathrm{diel}}a/2}\right)}{\left(\omega\mu_0\sigma_s - k_z^{\mathrm{diel}}\right)e^{ik_z^{\mathrm{diel}}a/2} - \left(\omega\mu_0\sigma_s + k_z^{\mathrm{diel}}\right)e^{-ik_z^{\mathrm{diel}}a/2}}, \tag{1}$$

$$\sigma_e^{\mathrm{TE}} = \sigma_s - \frac{k_z^{\mathrm{diel}}}{\omega\mu_0}\frac{e^{ik_z^{\mathrm{diel}}a/2} - e^{-ik_z^{\mathrm{diel}}a/2}}{e^{ik_z^{\mathrm{diel}}a/2} + e^{-ik_z^{\mathrm{diel}}a/2}}, \tag{2}$$

$$\sigma_m^{\mathrm{TM}} = \frac{k_z^{\mathrm{diel}}\left(e^{ik_z^{\mathrm{diel}}a/2} - e^{-ik_z^{\mathrm{diel}}a/2}\right)}{\left(k_z^{\mathrm{diel}}\sigma_s - \omega\varepsilon_0\varepsilon_r\right)e^{ik_z^{\mathrm{diel}}a/2} - \left(k_z^{\mathrm{diel}}\sigma_s + \omega\varepsilon_0\varepsilon_r\right)e^{-ik_z^{\mathrm{diel}}a/2}}, \tag{3}$$

and

$$\sigma_e^{\mathrm{TM}} = \sigma_s - \frac{\omega\varepsilon_0\varepsilon_r}{k_z^{\mathrm{diel}}}\frac{e^{ik_z^{\mathrm{diel}}a/2} - e^{-ik_z^{\mathrm{diel}}a/2}}{e^{ik_z^{\mathrm{diel}}a/2} + e^{-ik_z^{\mathrm{diel}}a/2}}, \tag{4}$$

where $\bar{k}^{\mathrm{diel}} = \hat{x}k_x + \hat{z}k_z^{\mathrm{diel}}$ is the wave vector of light within the dielectric slab, $|k^{\mathrm{diel}}| = \sqrt{\varepsilon_r}k_0$, and $k_0 = \omega/c$ is the wave vector of light in free space. The analytical calculations in this work are actually applicable for both lossless and lossy systems. For lossy systems, these conductivities are complex numbers, of which the real part characterizes the material loss. For conceptual brevity, the whole system below is considered to be lossless. As such, $\sigma_{e,m}^{\mathrm{TE}}$ and $\sigma_{e,m}^{\mathrm{TM}}$ are pure imaginary numbers. According to Eqs. (1) through (4), arbitrary magnetic and electric surface conductivities can, in

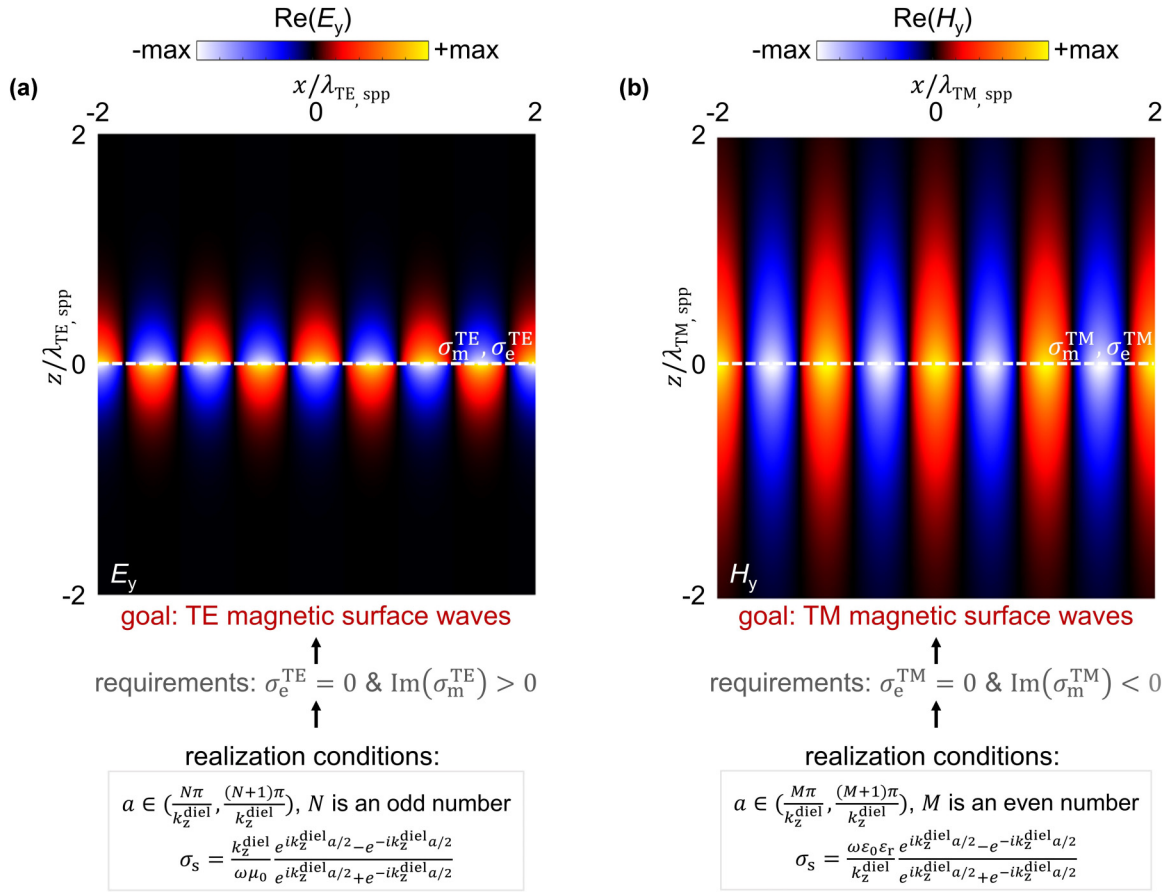

FIG. 2. Exotic plasmonic response at the optical interface only with a magnetic surface conductivity. Here, $\sigma_e^{TE,TM} = 0$, and the other structural setup is the same as Fig. 1. (a) Field distribution of TE magnetic surface waves if the interface has $\mathrm{Im}(\sigma_m^{TE}) > 0$. (b) Field distribution of TM magnetic surface waves if the optical interface has $\mathrm{Im}(\sigma_m^{TM}) < 0$. The wavelength of TE or TM surface waves [namely, surface plasmon polaritons (spp's)] is denoted as $\lambda_{TE,spp}$ and $\lambda_{TM,spp}$, respectively. Here, and in the following figures, the working frequency of 2 THz is chosen.

principle, be achieved, for example, by engineering the slab thickness and the electric surface conductivity of nonmagnetic metasurfaces. With this fancy capability enabled by vertical heterostructures, we now proceed to discuss some intriguing plasmonic and photonic phenomena emerging at optical interfaces with magnetic surface conductivity.

Figure 2 shows that under specific circumstances, the optical interface only with a magnetic surface conductivity (namely, in the absence of electric surface conductivity) can support the propagation of magnetic surface waves. Without loss of generality, the dispersion of surface waves at an optical interface with magnetic and electric surface conductivities is governed by

$$\left(k_z^{TE} + \omega\mu_0\sigma_e^{TE}\right) \cdot \left(1 + k_z^{TE} \cdot \frac{\sigma_m^{TE}}{\omega\mu_0}\right) = 0 \tag{5}$$

and

$$\left(1 + k_z^{TM} \cdot \frac{\sigma_e^{TM}}{\omega\varepsilon_0}\right)\left(k_z^{TM} + \sigma_m^{TM}\omega\varepsilon_0\right) = 0, \tag{6}$$

where $k_z^{TE,TM} = \sqrt{k_0^2 - (k_{||}^{TE,TM})^2}$ and $k_{||}^{TE,TM}$ are the components of the wave vector perpendicular and parallel to the interface, respectively. From Eqs. (5) and (6), the existence of magnetic surface waves is only determined by σ_m, regardless of σ_e. That is, the optical interface supports TE (TM) magnetic surface waves if $\mathrm{Im}(\sigma_m^{TE}) > 0$ ($\mathrm{Im}(\sigma_m^{TM}) < 0$). Similarly, σ_e plays a determinant role for the existence of electric surface waves. For brevity, the existence conditions for these magnetic and electric surface waves are summarized in Fig. 1(b).

Moreover, Eqs. (5) and (6) indicate that if $\sigma_e^{TE,TM} = 0$ and $\mathrm{Im}(\sigma_m^{TE}) > 0$ (or $\mathrm{Im}(\sigma_m^{TM}) < 0$), the optical interface would only support magnetic surface waves, without the appearance of electric surface waves. While this knowledge, along with Eqs. (5) and (6), is widely known to the community of plasmonics (see, for example, in Ref. [26]), how to create the optical interface only with a required magnetic surface conductivity remains elusive. We show in Fig. 2 that these conditions can be realized through the judicious design of vertical heterostructures.

Figure 2(a) shows TE magnetic surface waves supported at an optical interface that only has a magnetic surface conductivity with $\mathrm{Im}(\sigma_m^{TE}) > 0$. As can be seen from Eq. (2), we have $\sigma_e^{TE} = 0$ for TE waves, if the nonmagnetic metasurface has an electric surface conductivity of $\sigma_s = \frac{k_z^{diel}}{\omega\mu_0} \frac{e^{ik_z^{diel}a/2} - e^{-ik_z^{diel}a/2}}{e^{ik_z^{diel}a/2} + e^{-ik_z^{diel}a/2}}$, which can be realizable via regular design

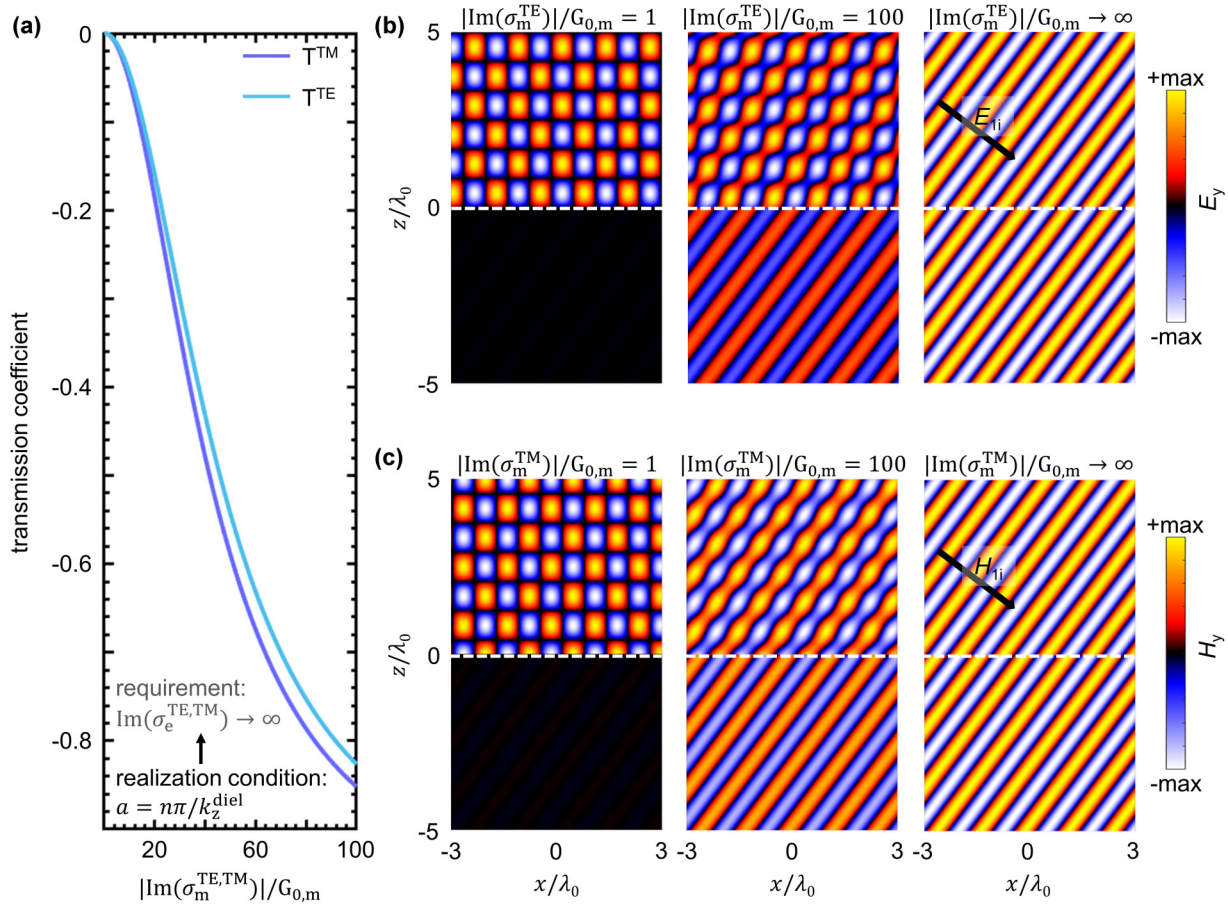

FIG. 3. Exotic transmission at the optical interface with magnetic and electric surface conductivities. The structural setup is the same as Fig. 1. Here we discuss the case with $|\sigma_e^{\mathrm{TE,\ TM}}| \to \infty$ under the incidence of either TE or TM waves with $\sin\theta_i = 0.8$. (a) Transmission coefficient T^{TE} (T^{TM}) as a function of $|\mathrm{Im}(\sigma_m^{\mathrm{TE}})|$ ($|\mathrm{Im}(\sigma_m^{\mathrm{TM}})|$). (b) Total field distribution under the incidence of TE waves. (c) Total field distribution under the incidence of TM waves. The white dashed line in (b) and (c) stands for the designed optical interface.

methodologies for metasurfaces [17–19]. By substituting this specific σ_s into Eq. (1), $\sigma_m^{\mathrm{TE}} = -i \cdot \frac{\omega\mu_0}{k_z^{\mathrm{diel}}(\tan\frac{k_z^{\mathrm{diel}}a}{2} + \cot\frac{k_z^{\mathrm{diel}}a}{2})}$ is obtained. Correspondingly, if the dielectric slab has a thickness of $a \in (\frac{N\pi}{k_z^{\mathrm{diel}}}, \frac{(N+1)\pi}{k_z^{\mathrm{diel}}})$ (N is an odd number), we further have $\mathrm{Im}(\sigma_m^{\mathrm{TE}}) > 0$, which is exactly the condition for TE magnetic surface waves. In Fig. 2(a), $a = \frac{1.5\pi}{k_z^{\mathrm{TE}}}$ and $\sigma_s = -19.77iG_{0,e}$ are applied in the vertical heterostructure, and then we have $\sigma_e^{\mathrm{TE}} = 0$, $\sigma_m^{\mathrm{TE}} = 48.36iG_{0,m}$, and $k_{||}^{\mathrm{TE}} = 1.34k_0$ for TE magnetic surface waves, where $G_{0,e} = e^2/4\hbar$ is the universal electric surface conductivity and $G_{0,m} = \frac{\mu_0}{\varepsilon_0}G_{0,e}$.

Similarly, Fig. 2(b) shows the propagation of TM magnetic surface waves at the optical interface that only has a magnetic surface conductivity with $\mathrm{Im}(\sigma_m^{\mathrm{TM}}) < 0$ by exploiting vertical heterostructures. From Eqs. (3) and (4), $\sigma_e^{\mathrm{TM}} = 0$ and $\sigma_m^{\mathrm{TM}} = -i \cdot \frac{k_z^{\mathrm{diel}}}{\omega\varepsilon_0\varepsilon_r(\tan\frac{k_z^{\mathrm{diel}}a}{2} + \cot\frac{k_z^{\mathrm{diel}}a}{2})}$, if the nonmagnetic metasurface in the vertical heterostructure has an electric surface conductivity of $\sigma_s = \frac{\omega\varepsilon_0\varepsilon_r}{k_z^{\mathrm{diel}}}\frac{e^{ik_z^{\mathrm{diel}}a/2} - e^{-ik_z^{\mathrm{diel}}a/2}}{e^{ik_z^{\mathrm{diel}}a/2} + e^{-ik_z^{\mathrm{diel}}a/2}}$. We further have $\mathrm{Im}(\sigma_m^{\mathrm{TM}}) < 0$, if the dielectric slab in the vertical heterostructure has a thickness of $a \in (\frac{M\pi}{k_z^{\mathrm{diel}}}, \frac{(M+1)\pi}{k_z^{\mathrm{diel}}})$ (M is an even number). In Fig. 2(d), $a = \frac{0.5\pi}{k_z^{\mathrm{TM}}}$ and $\sigma_s = 90.63iG_{0,e}$ are used for illustration; correspondingly, we have $\sigma_e^{\mathrm{TM}} = 0$, $\sigma_m^{\mathrm{TE}} = -10.59iG_{0,m}$, and $k_{||}^{\mathrm{TM}} = 1.03k_0$ for TM magnetic surface waves.

Upon close inspection of Eqs. (1) through (4), $\sigma_e^{\mathrm{TE,\ TM}}$ and $\sigma_m^{\mathrm{TE,\ TM}}$ can also be infinite under specific circumstances. To be specific, if $a = \frac{n\pi}{k_z^{\mathrm{diel}}}$ (n is an odd number), we have $\mathrm{Im}(\sigma_e^{\mathrm{TE,\ TM}}) \to \infty$ according to Eqs. (2) and (4), and $|\sigma_m^{\mathrm{TE,TM}}| = |\frac{1}{\sigma_s}|$ according to Eqs. (1) and (3). Furthermore, if $\sigma_s = 0$ (namely, the vertical heterostructure in Fig. 1 becomes a bare dielectric slab), $\mathrm{Im}(\sigma_m^{\mathrm{TE,TM}}) \to \infty$. Note that the optical interface with $\mathrm{Im}(\sigma_m^{\mathrm{TE,TM}}) \to \infty$ has been rarely explored due to the weak magnetic response available in nature, and it can give rise to some exotic photonic responses, as shown in Fig. 3.

Figure 3(a) shows the transmission of light through the optical interface as a function of $|\mathrm{Im}(\sigma_m^{\mathrm{TE,TM}})|$, under the extreme scenario of $\mathrm{Im}(\sigma_e^{\mathrm{TE,\ TM}}) \to \infty$ and with a fixed incident angle θ_i (e.g., $\sin\theta_i = 0.8$ used in the calculation). If $|\mathrm{Im}(\sigma_m^{\mathrm{TE,TM}})| \to 0$, total reflection happens [Fig. 3(a)–3(c)]. The transmittance $|T^{\mathrm{TE,TM}}|^2$ increases with $|\mathrm{Im}(\sigma_m^{\mathrm{TE,TM}})|$, and it reaches unity if $|\mathrm{Im}(\sigma_m^{\mathrm{TE,TM}})| \to \infty$ [Fig. 3(a)]. When

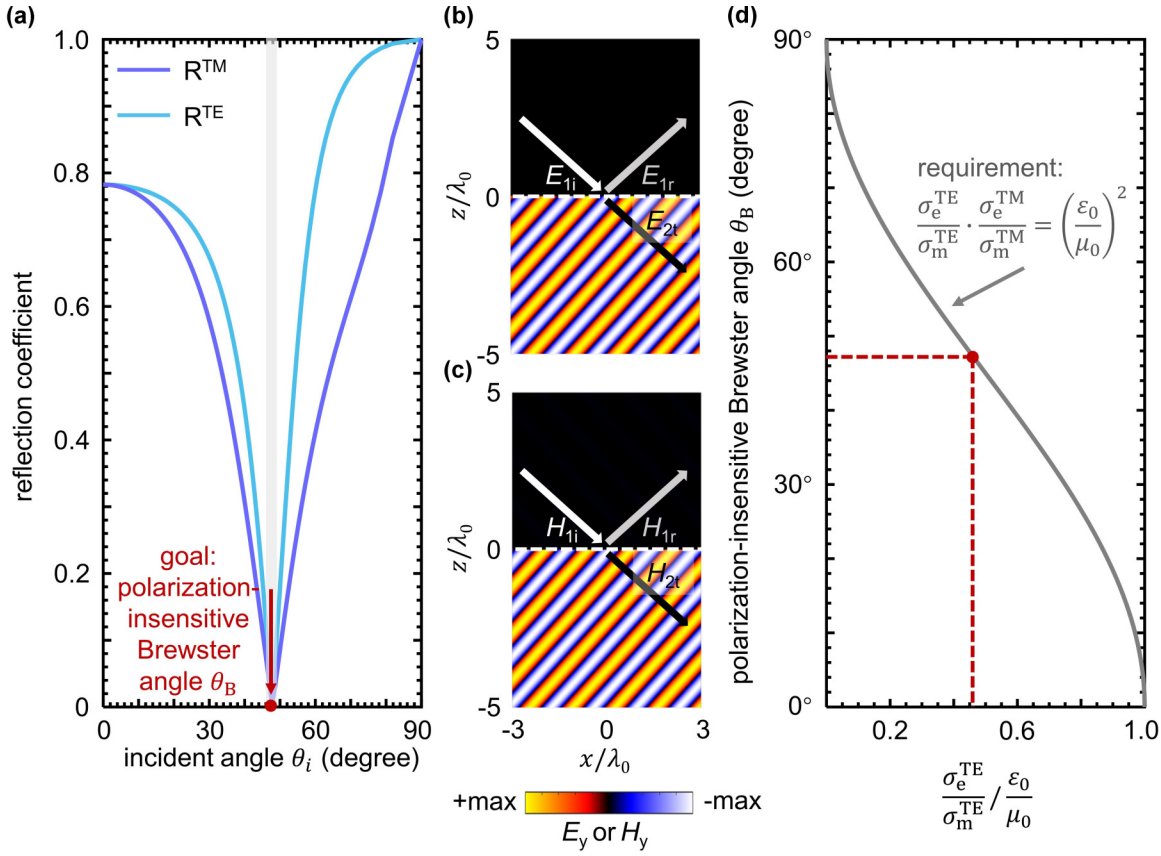

FIG. 4. Exotic reflection at the optical interface with magnetic and electric surface conductivities. The structural setup is the same as Fig. 1. (a) Reflection coefficients for TE and TM waves as a function of the incident angle. The polarization-insensitive Brewster angle occurs at $\theta_B = 47.7^o$. (b) and (c) Corresponding reflected and transmitted field distributions for TE or TM waves if the incident angle is $\theta_i = \theta_B = 47.7^o$. For clarity, the incident field is removed. The white dashed line in (b) and (c) stands for the designed optical interface. (d) Polarization-insensitive Brewster angle as a function of $\frac{\sigma_e^{TE}}{\sigma_m^{TE}} / \frac{\varepsilon_0}{\mu_0}$. The polarization-sensitive Brewster angle in (a) is highlighted as a red dot in (d).

perfect transmittance occurs, there is an abrupt phase change between the incident and the transmitted waves at the designed interface [Fig. 3(b) and 3(c)], since $T^{TE,TM} = -1$ [Fig. 3(a)].

We now turn to analyze another exotic photonic response at the optical interface with both magnetic and electric surface conductivities. We reveal in Fig. 4 that such an optical interface can support a polarization-insensitive Brewster effect, which is in drastic contrast to the extensively studied phenomenon of a polarization-sensitive Brewster effect [27–29]. By allowing the reflection coefficients R^{TE} and R^{TM} to be zero (Supplemental Material Sec. S2 [25]), the condition for the Brewster effect is obtained as

$$\frac{\sigma_e^{TE}}{\sigma_m^{TE}} = \frac{\varepsilon_0}{\mu_0} \cdot \cos^2\theta_{B,TE} \tag{7}$$

and

$$\frac{\sigma_e^{TM}}{\sigma_m^{TM}} = \frac{\varepsilon_0}{\mu_0} \cdot \frac{1}{\cos^2\theta_{B,TM}} \tag{8}$$

where $\theta_{B,TE}$ and $\theta_{B,TM}$ represent the Brewster angle for TE and TM waves, respectively. From Eqs. (7) and (8), TE waves have the Brewster effect only if $\frac{\sigma_e^{TE}}{\sigma_m^{TE}} / \frac{\varepsilon_0}{\mu_0} \in [0,\ 1]$, while the Brewster effect for TM waves would occur only if $\frac{\sigma_e^{TM}}{\sigma_m^{TM}} / \frac{\varepsilon_0}{\mu_0} \in [1, \infty]$; see the brief summary in Fig. 1(b).

Generally, if $\frac{\sigma_e^{TE}}{\sigma_m^{TE}} \cdot \frac{\sigma_e^{TM}}{\sigma_m^{TM}} \neq (\frac{\varepsilon_0}{\mu_0})^2$, we have $\theta_{B,TE} \neq \theta_{B,TM}$, according to Eqs. (7) and (8); that is, the Brewster effect would happen at different Brewster angles for waves with different polarizations, and it is thus polarization sensitive. However, if $\frac{\sigma_e^{TE}}{\sigma_m^{TE}} \cdot \frac{\sigma_e^{TM}}{\sigma_m^{TM}} = (\frac{\varepsilon_0}{\mu_0})^2$, we would simultaneously have $R^{TE} = R^{TM} = 0$ at the Brewster angle of $\theta_{B,TE} = \theta_{B,TM} = \theta_B$, as exemplified in Fig. 4(a)–4(c). Correspondingly, the Brewster effect for TE and TM waves occurs at the same Brewster angle and becomes polarization insensitive. Note that the condition for a polarization-insensitive Brewster effect can be readily achieved by exploiting the vertical heterostructure. For example, when $\sigma_s = 65.91iG_{0,e}$ and $a = 0.1$ mm are used, this condition is fulfilled at 2 THz, and we have a polarization-insensitive Brewster angle of $\theta_B = 47.7^o$ in Fig. 4(a). Moreover, Fig. 4(d) shows that the polarization-insensitive Brewster angle θ_B can vary from 0^o to 90^o by judiciously engineering $\frac{\sigma_e^{TE}}{\sigma_m^{TE}}$ and $\frac{\sigma_e^{TM}}{\sigma_m^{TM}}$. For example, when $\frac{\sigma_e^{TE}}{\sigma_m^{TE}} = \frac{\sigma_e^{TM}}{\sigma_m^{TM}} = \frac{\varepsilon_0}{\mu_0}$, we have $\theta_B = 0^o$. In addition, Supplemental

Material Fig. S4 [25] shows that the polarization-insensitive Brewster effect can be approximately preserved under a relatively small material loss.

III. CONCLUSION

In conclusion, we have revealed that vertical heterostructures have the capability to provide a universal platform for the flexible design of effective optical interfaces with on-demand magnetic surface conductivities, whose values are, in principle, unbounded. This unique property allows us to uncover some intriguing and hidden plasmonic and photonic phenomena at the optical interface with a magnetic surface conductivity. Particularly, we have found the specific conditions for optical interfaces to achieve the polarization-insensitive Brewster effect, and we have demonstrated a feasible scheme to construct the optical interface that only has a magnetic surface conductivity and that can only support the propagation of magnetic surface waves. Due to the flexibility of our scheme to tailor the effective magnetic response, our work may trigger many other fundamental studies on optical systems with magnetic responses, such as the free-electron radiation [30–32] from magnetic photonic crystals and the near-field directionality [32–36] from magnetic interfaces.

ACKNOWLEDGMENTS

The work was sponsored by the National Natural Science Foundation of China (Grants No. 61625502, No. 11961141010, No. 61975176, and No. 62175212), the Top-Notch Young Talents Program of China, the Excellent Young Scientists Fund Program (Overseas) of China, the Fundamental Research Funds for the Central Universities (Grant No. 2021FZZX001-19), and the Zhejiang University Global Partnership Fund.

[1] H. Kroemer, Quasielectric fields and band offsets: Teaching electrons new tricks, Rev. Mod. Phys. **73**, 783 (2001).
[2] The interface is still the device, Nat. Mater. **11**, 91 (2012).
[3] F. Monticone, N. M. Estakhri, and A. Alù, Full Control of Nanoscale Optical Transmission with a Composite Metascreen, Phys. Rev. Lett. **110**, 203903 (2013).
[4] V. G. Ataloglou, M. Chen, M. Kim, and A. G. V. Eleftheriades, Microwave Huygens' metasurfaces: Fundamentals and applications, IEEE J. Microwaves **1**, 374 (2021).
[5] C. Pfeiffer and A. Grbic, Metamaterial Huygens' Surfaces: Tailoring Wave Fronts with Reflectionless Sheets, Phys. Rev. Lett. **110**, 197401 (2013).
[6] L. Thiel, Z. Wang, M. A. Tschudin, D. Rohner, I. Gutiérrez-Lezama, N. Ubrig, M. Gibertini, E. Giannini, A. F. Morpurgo, and P. Maletinsky, Probing magnetism in 2D materials at the nanoscale with single-spin microscopy, Science **364**, 973 (2019).
[7] B. Huang, G. Clark, D. R. Klein, D. MacNeill, E. Navarro-Moratalla, K. L. Seyler, N. Wilson, M. A. McGuire, D. H. Cobden, D. Xiao, W. Yao, P. Jarillo-Herrero, and X. Xu, Electrical control of 2D magnetism in bilayer CrI_3, Nat. Nanotechnol. **13**, 544 (2018).
[8] Z. Qiu, M. Holwill, T. Olsen, P. Lyu, J. Li, H. Fang, H. Yang, M. Kashchenko, K. S. Novoselov, and J. Lu, Visualizing atomic structure and magnetism of 2D magnetic insulators via tunneling through graphene, Nat. Commun. **12**, 70 (2021).
[9] D. O. Ignatyeva, D. Karki, A. A. Voronov, M. A. Kozhaev, D. M. Krichevsky, A. I. Chernov, M. Levy, and V. I. Belotelov, All-dielectric magnetic metasurface for advanced light control in dual polarizations combined with high-Q resonances, Nat. Commun. **11**, 5487 (2020).
[10] A. Howes, W. Wang, I. Kravchenko, and J. Valentine, Dynamic transmission control based on all-dielectric Huygens metasurfaces, Optica **5**, 787 (2018).
[11] A. M. H. Wong and G. V. Eleftheriades, Perfect Anomalous Reflection with a Bipartite Huygens' Metasurface, Phys. Rev. X **8**, 011036 (2018).
[12] A. L. Holsteen, A. F. Cihan, and M. L. Brongersma, Temporal color mixing and dynamic beam shaping with silicon metasurfaces, Science **365**, 257 (2019).
[13] J. Li, P. Yu, S. Zhang, and N. Liu, A reusable metasurface template, Nano Lett. **20**, 6845 (2020).
[14] P. Thureja, G. K. Shirmanesh, K. T. Fountaine, R. Sokhoyan, M. Grajower, and H. A. Atwater, Array-level inverse design of beam steering active metasurfaces, ACS Nano **14**, 15042 (2020).
[15] C.-H. Lin, Y.-S. Chen, J.-T. Lin, H. C. Wu, H.-T. Kuo, C.-F. Lin, P. Chen, and P. C. Wu, Automatic inverse design of high-performance beam-steering metasurfaces via genetic-type tree optimization, Nano Lett. **21**, 4981 (2021).
[16] S. Boroviks, R. A. Deshpande, N. A. Mortensen, and S. I. Bozhevolnyi, Multifunctional metamirror: Polarization splitting and focusing, ACS Photonics **5**, 1648 (2018).
[17] O. Luukkonen, C. Simovski, G. Granet, G. Goussetis, D. Lioubtchenko, A. V. Raisanen, and S. A. Tretyakov, Simple and accurate analytical model of planar grids and high-impedance surfaces comprising metal strips or patches, IEEE Trans. Antennas Propag. **56**, 1624 (2008).
[18] Y. R. Padooru, A. B. Yakovlev, P.-Y. Chen, and A. Alù, Analytical modeling of conformal mantle cloaks for cylindrical objects using sub-wavelength printed and slotted arrays, J. Appl. Phys. **112**, 034907 (2012).
[19] C. Qian, X. Lin, Y. Yang, X. Xiong, H. Wang, E. Li, I. Kaminer, B. Zhang, and H. Chen, Experimental Observation of Superscattering, Phys. Rev. Lett. **122**, 063901 (2019).
[20] S. A. Mikhailov and K. Ziegler, New Electromagnetic Mode in Graphene, Phys. Rev. Lett. **99**, 016803 (2007).
[21] X. Lin, N. Rivera, J. J. López, I. Kaminer, H. Chen, and M. Soljačić, Tailoring the energy distribution and loss of 2D plasmons, New J. Phys. **18**, 105007 (2016).
[22] V. P. Gusynin, S. G. Sharapov, and J. P. Carbotte, Unusual Microwave Response of Dirac Quasiparticles in Graphene, Phys. Rev. Lett. **96**, 256802 (2006).
[23] G. T. Papadakis, D. Fleischman, A. Davoyan, P. Yeh, and H. A. Atwater, Optical magnetism in planar metamaterial heterostructures, Nat. Commun. **9**, 296 (2018).
[24] K. E. Ballantine and J. Ruostekoski, Optical Magnetism and Huygens' Surfaces in Arrays of Atoms Induced by Cooperative Responses, Phys. Rev. Lett. **125**, 143604 (2020).

[25] See Supplemental Material at http://link.aps.org/supplemental/10.1103/PhysRevB.106.035304 for the derivation of electric and magnetic surface conductivities, the derivation of reflection and transmission at optical interfaces with electric and magnetic surface conductivities, the verification of the equivalence between the effective optical interface and the realistic vertical heterostructure, and a discussion on the influence of material loss on the polarization-insensitive Brewster effect.

[26] X. Lin, Z. Liu, T. Stauber, G. Gómez-Santos, F. Gao, H. Chen, B. Zhang, and T. Low, Chiral Plasmons with Twisted Atomic Bilayers, Phys. Rev. Lett. **125**, 077401 (2020).

[27] R. Paniagua-Domínguez, Y. F. Yu, A. E. Miroshnichenko, L. A. Krivitsky, Y. H. Fu, V. Valuckas, L. Gonzaga, Y. T. Toh, A. Y. S. Kay, B. Luk'yanchuk, and A. I. Kuznetsov, Generalized Brewster effect in dielectric metasurfaces, Nat. Commun. **7**, 10362 (2016).

[28] X. Lin, Y. Shen, I. Kaminer, H. Chen, and M. Soljačić, Transverse-electric Brewster effect enabled by nonmagnetic two-dimensional materials, Phys. Rev. A **94**, 023836 (2016).

[29] J. A. Kong, *Electromagnetic Wave Theory* (EMW Publishing, Cambridge, 2008).

[30] X. Lin, I. Kaminer, X. Shi, F. Gao, Z. Yang, Z. Gao, H. Buljan, J. D. Joannopoulos, M. Soljačić, H. Chen, and B. Zhang, Splashing transients of 2D plasmons launched by swift electrons, Sci. Adv. **3**, e1601192 (2017).

[31] X. Lin, S. Easo, Y. Shen, H. Chen, B. Zhang, J. D. Joannopoulos, M. Soljačić, and I. Kaminer, Controlling Cherenkov angles with resonance transition radiation, Nat. Phys. **14**, 816 (2018).

[32] J. Chen, H. Chen, and X. Lin, Photonic and plasmonic transition radiation from graphene, J. Opt. **23**, 034001 (2021).

[33] F. J. Rodríguez-Fortuño, G. Marino, P. Ginzburg, D. O'Connor, A. Martínez, G. A. Wurtz, and A. V. Zayats, Near-field interference for the unidirectional excitation of electromagnetic guided modes, Science **340**, 328 (2013).

[34] M. F. Picardi, A. V. Zayats, and F. J. Rodríguez-Fortuño, Janus and Huygens Dipoles: Near-Field Directionality Beyond Spin-Momentum Locking, Phys. Rev. Lett. **120**, 117402 (2018).

[35] Y. Long, J. Ren, Z. Guo, H. Jiang, Y. Wang, Y. Sun, and H. Chen, Designing All-Electric Subwavelength Metasources for Near-Field Photonic Routings, Phys. Rev. Lett. **125**, 157401 (2020).

[36] Y. Zhong, X. Lin, J. Jiang, Y. Yang, G.-G. Liu, H. Xue, T. Low, H. Chen, and B. Zhang, Toggling near-field directionality via polarization control of surface waves, Laser Photonics Rev. **15**, 2000388 (2021).